



Lab-scale experiments and model analyses for bacterial removal in flow-through columns containing dolomite

Seong-Jik Park^a, Chang-Gu Lee^b, Song-Bae Kim^{c,*}

^aDepartment of Bioresources and Rural Systems Engineering, Hankyong National University, Anseong 456-749, Korea

^bEnvironmental Functional Materials & Biocolloids Laboratory, Seoul National University, Seoul 151-921, Korea

^cDepartment of Rural Systems Engineering, Seoul National University, Seoul 151-921, Korea
Tel. +82 2 880 4587; email: songbkim@snu.ac.kr

Received 4 April 2013; Accepted 7 June 2013

ABSTRACT

The aim of this study was to investigate the removal of bacteria (*Bacillus subtilis* ATCC 6633) from aqueous solutions using dolomite as a filter medium. Column experiments were performed in step injection mode under various conditions of influent bacterial concentration (0.5–2.0 g/L), flow rate (0.5–1.5 mL/min), and column length (10–30 cm). The highest percentage bacterial removal (Re) of $75.2 \pm 1.6\%$ was obtained under the following conditions: influent bacterial concentration = 1.0 g/L; flow rate = 0.5 mL/min; column length = 20 cm. The highest column capacity for bacterial removal (q_0) of 2.126 ± 0.067 mg/g was achieved using an influent bacterial concentration of 2.0 g/L, flow rate of 1.0 mL/min, and column length of 20 cm. Increasing the bacterial concentration and flow rate had a negative effect on Re , whereas the q_0 values were positively affected. Increasing the column length produced a positive effect on Re , whereas q_0 declined. Simulation of the breakthrough curves (BTCs) using the Adams–Bohart, Thomas, Yoon–Nelson, and dose-response kinetic models demonstrated that the Adams–Bohart model adequately reproduced the initial part of the BTC, whereas the Thomas and Yoon–Nelson models were suitable for describing the transient stage of the BTC between the breakthrough point and saturation point. Compared to the aforementioned models, the dose-response model produced an adequate simulation of the entire BTC. This study demonstrates the adequate performance of dolomite as a filter material for the removal of bacteria from aqueous solutions.

Keywords: Bacteria removal; Breakthrough curve; Column experiment; Dolomite; Kinetic model

1. Introduction

Adhesion of bacteria to dolomite, a carbonate mineral comprising a double carbonate of calcium and magnesium (CaCO_3 , MgCO_3), has been examined

by various researchers from two perspectives. The first relates to the use of bacteria as reagents for bioflotation and bioflocculation in mineral bioprocessing [1–3]. In this respect, bacteria can adhere to minerals and modify the properties of the mineral surfaces, thereby enhancing the separation selectivity of the

*Corresponding author.

minerals from associated impurities. The second concerns the adhesion of bacteria to dolomite in subsurface environmental systems [4,5]. During transport of bacteria through geological formations such as subsurface biobarriers, the migration of bacteria can be attenuated as a result of adhesion of bacteria to mineral surfaces.

For several decades, researchers have studied raw and treated dolomite as low-cost and environmentally friendly adsorbents for the removal of inorganic/organic contaminants and heavy metals [6–14]. For example, fluoride ions may be adsorbed onto dolomite by the formation of calcium fluoride precipitates and via ion-exchange processes [15]. Pentachlorophenol has also been effectively removed from aqueous systems using dolomite that was thermally treated at 1,000 °C [16]. Divalent heavy metals such as Ba^{2+} and Sr^{2+} have been adsorbed onto dolomite through cation exchange and surface complexation [17] and thermally modified dolomite has been effectively employed in the adsorption of a reactive dye [18]. However, there is a paucity of data related to the removal of bacteria using dolomite.

The removal of bacteria using dolomite as a filter medium is investigated herein. Column experiments were performed using various influent bacterial concentrations, flow rates, and column lengths. Breakthrough curves (BTCs) for the bacteria were obtained by monitoring the effluent, and the percentage removal and column capacity were quantified from these curves. In addition, four kinetic models were used to simulate the BTCs and to quantify the kinetic parameters.

2. Materials and methods

2.1. Bacteria and culture preparation

Bacillus subtilis ATCC 6633 obtained from the Korea Culture Center for Microorganisms was used in the experiments. The procedures for the bacterial preparation have been previously described [19] and are briefly outlined as follows: all glassware and materials used in this study were sterilized by autoclaving at 121 °C under 17.6 psi of pressure for 20 min. The bacteria were grown in LB medium (tryptone 10 g, yeast extract 5 g, NaCl 5 g in one liter of deionized water at pH 7.0) over a period of 84 h. The suspension was centrifuged at 4 °C and 10,000 rpm for 15 min. The supernatant was removed and replaced with deionized water to prevent further bacterial growth. Diluted bacteria were centrifuged again under the same conditions, washed three times with deionized water, and re-suspended in the solution to adjust the bacterial concentration.

The bacterial cell properties including morphology, surface charge, and hydrophobicity were analyzed. The cell size of *B. subtilis* was determined by means of cell images acquired via transmission electron microscopy (TEM) (JEM 1010, JEOL, Japan). The cell length and width were $1.67 \pm 0.31 \mu\text{m}$ and $0.77 \pm 0.07 \mu\text{m}$, respectively, which is equivalent to a diameter of $1.18 \pm 0.10 \mu\text{m}$. The zeta potential of the bacterial cells, measured with an electrophoretic light-scattering spectrophotometer (ELS-8000, Otsuka Electronics, Japan) was $-31.9 \pm 3.2 \text{ mV}$ (pH = 6.8, temperature = 25 °C, ionic strength $\approx 0 \text{ mM}$). The hydrophobicity of the bacteria was determined to be 3.4 ± 1.3 (hydrophilic) based on microbial adhesion to hydrocarbons (MATH) analysis using *n*-hexadecane.

2.2. Filter material

Dolomite (Seongshin Mining Corporation, Chungju, Korea) was used in the experiments. Prior to use, dolomite was prepared by mechanical sieving through US Standard Sieves No. 20 and No. 16 (grain size: 0.84–1.19 mm) and was washed twice with deionized water to remove surface impurities. The wet, filtered materials were autoclaved for 20 min at 17.6 psi, cooled to room temperature, and oven-dried at 105 °C for one day. Surface analysis of dolomite was carried out using field emission scanning electron microscopy (FESEM) and energy dispersive X-ray spectrometry (EDS) using a field emission scanning electron microscope (Supra 55VP, Carl Zeiss, Germany). The mineralogical and crystalline structural properties were examined using X-ray diffractometry (XRD, D8 Advance, Bruker, Germany) using $\text{CuK}\alpha$ radiation of 1.5406 Å at a scanning speed of 0.6 °/s. Infrared spectra were recorded on a Nicolet 6700 (Thermo Scientific, USA) Fourier transformed infrared (FTIR) spectrometer using KBr pellets.

2.3. Column experiments

Column experiments were performed using a Plexiglas column packed with dolomite. Each column experiment employed a separate column packed with dolomite by the tap-fill method. The experimental conditions are provided in Table 1. The influent concentrations of bacteria were 0.5, 1.0, and 2.0 g/L in the first set of experiments (Exps. 1–3). Prior to the experiments, the packed column (column length = 20 cm; inner diameter = 2.5 cm) was flushed upward using a high-performance liquid chromatography (HPLC) pump (Series II pump, Scientific Systems Inc., State College, PA, USA) operating at a rate of 1.0 mL/min using 10 bed volumes of artificial solution (0.014 g/L

Table 1
Column experimental conditions for bacteria removal in dolomite

Exp.	Influent conc. (g/L)	Flow rate (mL/min)	Column length (cm)	pH _{effluent}	EC _{effluent} (μS/cm)
1	0.5	1.0	20	7.75 ± 0.07	676.8 ± 5.4
2	1.0	1.0	20	7.84 ± 0.05	685.6 ± 4.8
3	2.0	1.0	20	7.71 ± 0.03	695.2 ± 6.3
4	1.0	0.5	20	7.85 ± 0.01	683.1 ± 5.9
5	1.0	1.5	20	7.92 ± 0.01	678.4 ± 3.5
6	1.0	1.0	10	7.64 ± 0.06	679.6 ± 3.3
7	1.0	1.0	30	8.07 ± 0.04	685.7 ± 5.5

of KNO₃, 0.321 g/L of MgSO₄·7H₂O, 0.112 g/L of CaSO₄·2H₂O, 0.044 g/L of NaCl, and 0.109 g/L of NaHCO₃) until steady-state flow conditions were established. The bacteria suspended in the artificial solution were then introduced downward into the packed column at the same flow rate in a step injection mode. The experiment was continued until a BTC plateau was obtained. In the column experiments, the “gram” unit was used for bacterial concentration instead of “CFU”. A bacterial mass concentration of 0.5 g/L corresponded to 1.5 × 10⁹ CFU/mL. Portions of the effluent were collected at regular intervals using an auto-collector (Retriever 500, Teledyne, City of Industry, CA, USA). Effluent samples were analyzed for bacterial concentration along with electrical conductivity (EC) and pH. Bacterial concentrations were determined by colony counts from the LD agar plates. EC was measured with an EC probe (815PDL, Istek, Korea) and the pH was measured with a pH probe (9107BN, Orion, USA). The second set of experiments (Exps. 4, 5) was performed by varying the flow rates (0.5, 1.5 mL/min) in the dolomite columns (column length = 20 cm; influent bacterial concentration = 1 g/L). The column length was varied (10, 30 cm) in the third set of experiments (Exps. 6, 7) conducted using flow rate = 1.0 mL/min and influent bacterial concentration = 1 g/L. All experiments were performed in duplicate and the average values were used for further data analysis.

2.4. Column data analysis

The total mass of bacteria injected into the column (m_{total}) during the experiment is calculated as:

$$m_{\text{total}} = \frac{C_0 Q t_{\text{total}}}{1,000} \quad (1)$$

where C_0 is the influent concentration of bacteria, Q is the volumetric flow rate, and t_{total} is the total flow time. The bacterial removal in the column at a given flow rate and influent bacterial concentration (q_{total}) is quantified as:

$$q_{\text{total}} = \frac{Q}{1000} \int_{t=0}^{t=t_{\text{total}}} (C_0 - C_t) dt \quad (2)$$

where C_t is the effluent bacterial concentration. The percentage removal of bacteria during the experiment (Re) is determined as:

$$Re = \left(\frac{q_{\text{total}}}{m_{\text{total}}} \right) \times 100 \quad (3)$$

The column capacity for bacterial removal per unit mass of filter medium (q_0) is calculated as:

$$q_0 = \frac{q_{\text{total}}}{X} \quad (4)$$

where X is the mass of filter medium in the column. The one-dimensional transport equation for bacteria can be described as:

$$\frac{\partial C_i}{\partial t} = D_i \frac{\partial^2 C_i}{\partial X^2} - v_i \frac{\partial C_i}{\partial X} - \lambda C_i \quad (5)$$

where C_i is the bacterial concentration in the aqueous phase, D_i is the hydrodynamic dispersion coefficient for bacteria, v_i is the velocity for bacteria, and λ is the removal rate coefficient. Parameters in the transport models were obtained by fitting the CXTFIT code [20] to the breakthrough data. The Damköhler number (D_a) was calculated from the removal rate coefficient (λ) using the following relationship:

$$D_a = \frac{\lambda L}{v_i} \quad (6)$$

where L = column length. Note that D_a is used in the data analysis instead of λ because of the interference of the bacterial velocity (v_i) on the estimation of λ with time-scale effect [21].

2.5. Kinetic model analysis

Adams–Bohart, Thomas, Yoon–Nelson, and dose-response models were used to simulate the dynamic behavior of the column packed with dolomite. These models are commonly used for column studies because of their lower complexity relative to other theoretical models. The Adams–Bohart model is given as [22]:

$$\frac{C_t}{C_0} = \exp\left(k_{AB}C_0t - k_{AB}N_0\frac{Z}{v}\right) \quad (7)$$

where k_{AB} is the rate constant, N_0 is the saturation concentration of bacteria, Z is the column length, and v is the linear velocity, calculated by dividing the flow rate by the column section area. The Thomas model is given as [23]:

$$\frac{C_t}{C_0} = \frac{1}{1 + \exp\left(\frac{k_{TH}q_0X}{Q} - k_{TH}C_0t\right)} \quad (8)$$

where k_{TH} is the rate constant. The Yoon–Nelson model is given as [24]:

$$\frac{C_t}{C_0} = \frac{1}{1 + \exp[(k_{YN}(\tau - t))]} \quad (9)$$

where k_{YN} is the rate constant and τ is the time required for 50% breakthrough of bacteria. Finally, the dose-response model is given as [25,26]:

$$\frac{C_t}{C_0} = 1 - \frac{1}{1 + \left(\frac{C_0Q_t}{q_0X}\right)^A} \quad (10)$$

where A is the constant of the dose-response model.

From a plot of C_t/C_0 against t at a given influent bacterial concentration, flow rate, column length adopting a nonlinear regression coefficient, the kinetic parameters including k_{AB} , N_0 , k_{TH} , q_0 , k_{YN} , τ , and A were determined. The coefficient of determination (R^2) and the standard error of estimate (SSE) were used to analyze the data and confirm the fit to the model for the column experiments. The expression for the calculation of SSE is given as:

$$SSE = \sqrt{\frac{\sum_{i=1}^n (y_c - y_e)_i^2}{n}} \quad (11)$$

where n is the number of experimental data points, y_c is the predicted data obtained from the model fit, and y_e is the experimental data.

3. Results and discussion

3.1. Characteristics of dolomite

The digital and FESEM images of dolomite used in the column experiments are shown in Fig. 1. The particles were white (Fig. 1(a)), and irregularly shaped

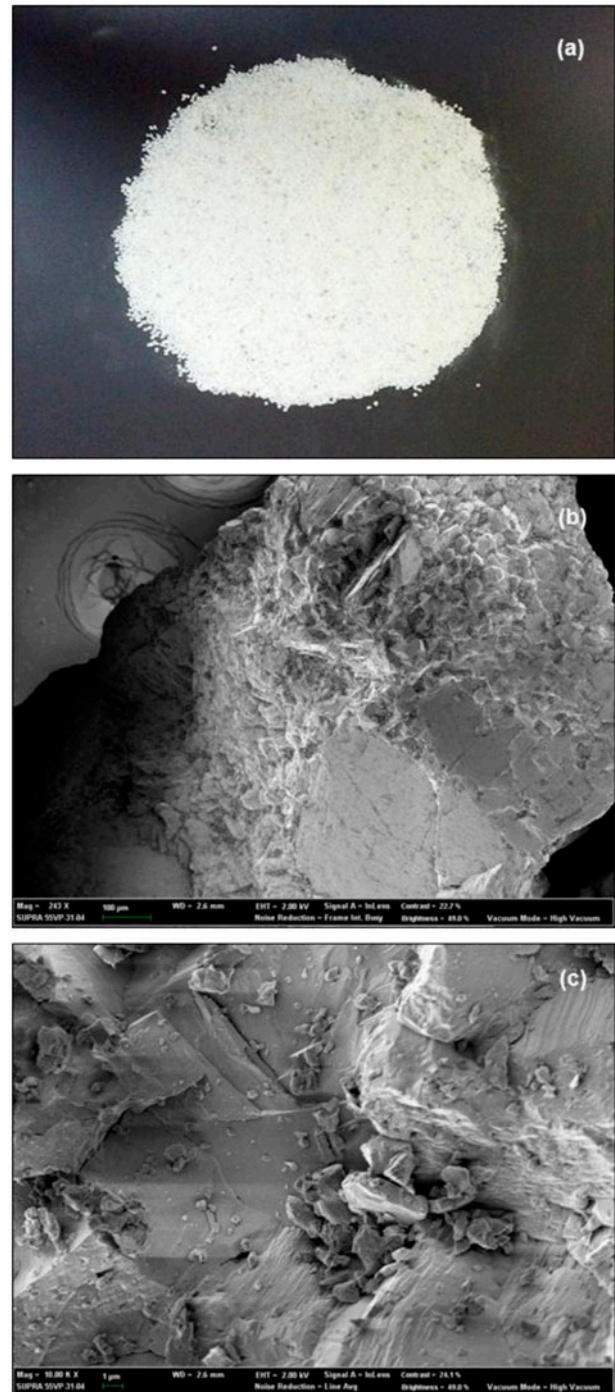


Fig. 1. Dolomite used in the experiments: (a) digital image; (b) field emission scanning electron microscopy (FESEM) image (bar = 100 μ m); (c) FESEM image (bar = 1 μ m).

(Fig. 1(b)) with a rough and heterogeneous surface (Fig. 1(c)). The EDS, XRD, and FTIR of dolomite are presented in Fig. 2. The presence of magnesium (Mg) was evidenced by peaks in the EDS pattern (Fig. 2(a)) at 1.254 and 1.295 keV, corresponding to $K\alpha$ and $K\beta$ X-ray signals, respectively, whereas peaks correspond-

ing to calcium (Ca) were observed at 0.341, 3.691, and 4.012 keV as $L\alpha$, $K\alpha$, and $K\beta$ signals, respectively. The XRD pattern (Fig. 2(b)) of the dolomite $[\text{CaMg}(\text{CO}_3)_2]$ was characterized by the peaks at $2\theta = 30.963$, 41.161, 44.987, 50.569, and 51.111, which are attributed to (104), (113), (202), (018), and (116) crystal planes of dolomite (JCPD standard: 36-0426). The FTIR spectrum (Fig. 2(c)) indicated the main bands of dolomite at 3,020, 2,627, 2,523, 1,821, 1,437, 880, and 728 cm^{-1} [27]. It was reported that the absorption bands at 3,020, 2,627, and 728 cm^{-1} were the characteristics of dolomite compared to calcite [28]. The band at 728 cm^{-1} was corresponded to the in-plane bending mode of carbonate (CO_3^{2-}) group [28,29]. In addition, the dolomite used in the column experiments had a particle size of 0.84–1.19 mm, bulk density of $1.730 \pm 0.045 \text{ g/cm}^3$, and porosity of 0.359 ± 0.016 .

3.2. Bacterial removal by dolomite

The BTCs from the column experiments and transport model fits are presented in Figs. 3 and 4, respectively. The experimental results and transport model parameters are summarized in Table 2. The BTCs obtained by varying the influent concentration of bacteria (Exps. 1–3, Table 1) are shown in Fig. 3(a). With increasing bacterial concentration, the BTCs became steeper and saturation was achieved more quickly. As the influent concentration increased from 0.5 to 2.0 g/L, the values of D_a decreased from 0.359 to 0.134. Also, the percentage removal (Re) decreased from 57.2 ± 1.0 to $27.7 \pm 0.9\%$, whereas the column capacity (q_0) increased from 0.998 ± 0.019 to $2.126 \pm 0.067 \text{ mg/g}$ (Fig. 5(a)). With increasing influent concentration of bacteria, the concentration gradient between the aqueous phase and the solid phase becomes larger, thereby increasing the driving force for bacterial adhesion to the adsorbents [30,31].

The BTCs obtained by varying the flow rates (Exps. 2, 4, and 5, Table 1) are presented in Fig. 3(b). Steeper BTCs, an earlier breakthrough point, and higher saturation concentration were observed with increasing flow rate (bacterial loading rate). As the flow rate increases, the contact time between the bacteria and the filter medium decreases, while the shear force on the surface of the filter medium increases [32,33]. In the current experiments, the empty bed contact time decreased from 70.5 to 23.5 min as the flow rate was increased from 0.5 to 1.5 mL/min (column length = 20 cm). As the flow rate increases, the BTC becomes steeper because the driving forces increase, leading to a decrease in the adsorption zone length [31]. Increasing the flow rate from 0.5 to 1.5 mL/min decreased the values of D_a from 0.361 to

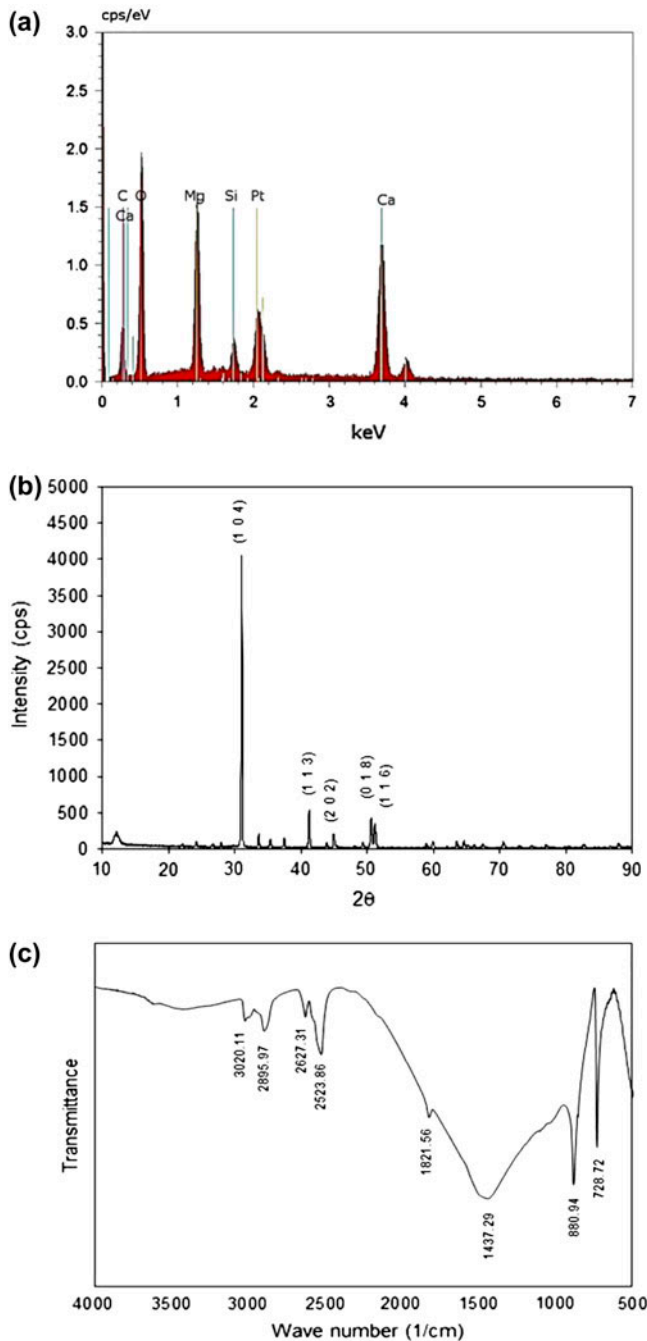


Fig. 2. Energy dispersive X-ray spectrometry (EDS) pattern (a); X-ray diffraction (XRD) pattern (b); Fourier transformed infrared (FTIR) spectra (c) of dolomite used in the experiments.

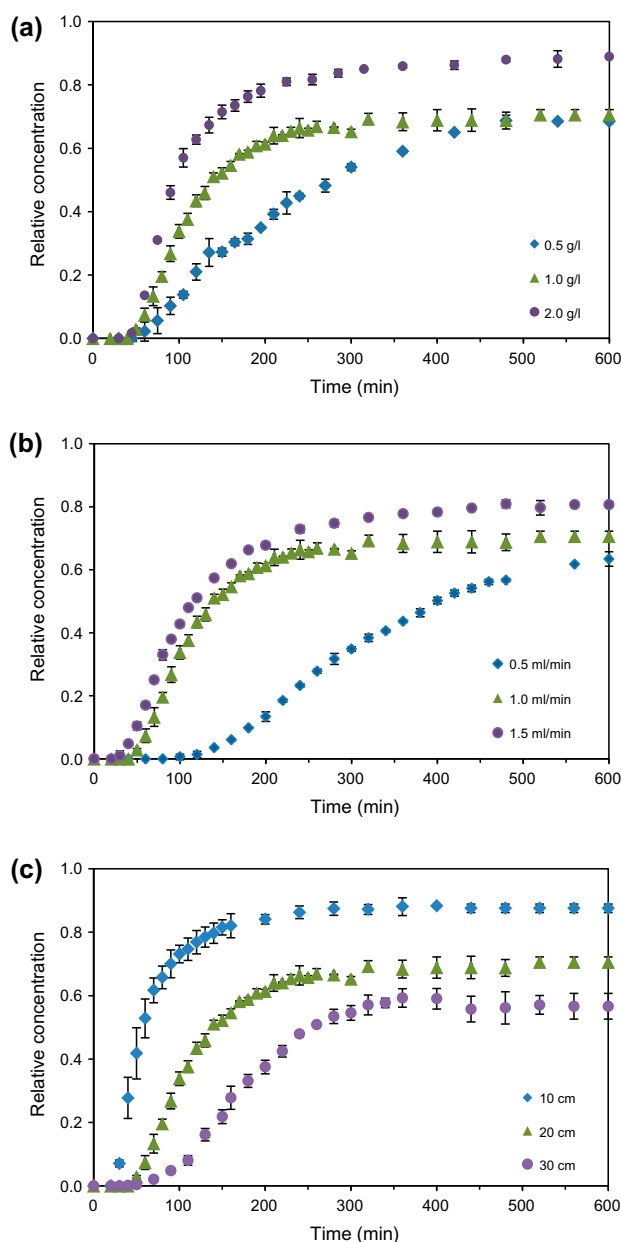


Fig. 3. Bacterial breakthrough curves and transport model fits with variations of (a) influent bacterial concentration; (b) flow rate; (c) column length. Experimental conditions are provided in Table 1.

0.190. Also, the values of Re decreased from 75.2 ± 1.6 to $36.7 \pm 0.1\%$, whereas the values of q_0 increased from 1.315 ± 0.062 to 1.922 ± 0.009 mg/g (Fig. 5(b)).

The BTCs obtained by varying the column length (Exps. 2, 6, and 7, Table 1) are provided in Fig. 3(c). Increasing the column length, i.e. the bed height, produced BTCs with lower saturated effluent concentrations and later breakthrough points. The longer column length leads to more dispersed BTCs, that is, increasing the column length broadens the mass

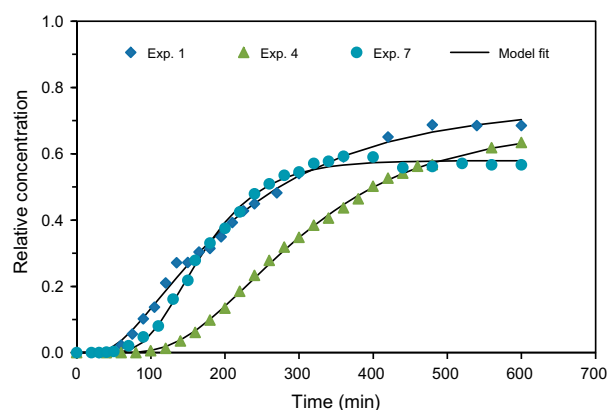


Fig. 4. Transport model fits to bacterial breakthrough curves. Transport model parameters are provided in Table 2.

transfer zone, resulting in a decrease of the BTC slope [31]. Increasing the column length also decreased the concentration of bacteria in the effluent as a result of an increase in the contact time for bacterial adhesion to dolomite. Note that the empty bed contact time increased from 98.2 to 294.5 min as the column length was increased from 10 to 30 cm. As the column length was increased from 10 to 30 cm, the values of D_a increased from 0.123 to 0.524. Also, the Re values increased from 22.8 ± 0.6 to $60.9 \pm 2.4\%$, whereas the q_0 values decreased from 1.706 ± 0.051 to 1.427 ± 0.058 mg/g (Fig. 5(c)).

Supplementary comparisons of the bacterial removal using dolomite, quartz sand, and granular activated carbon were undertaken in pulse injection mode using the column (column length = 20 cm; inner diameter = 2.5 cm) under the following conditions: influent bacterial concentration = 1.0 g/L; flow rate = 0.5 mL/min; injection time = 40 min. The results indicated that the percentage bacterial removal was ranked in the order: dolomite ($87.5 \pm 1.0\%$) > granular activated carbon ($44.2 \pm 0.1\%$) > quartz sand ($14.4 \pm 2.2\%$). Dolomite showed better performance in the bacterial removal than conventional filter materials such as quartz sand and granular activated carbon.

The bacterial removal by dolomite can be explained in terms of the Derjaguin–Landau–Verwey–Overbeek (DLVO) theory. Bacterial adhesion to particles is complex and is dependent on the van der Waals forces and electric double-layer interactions. The attractive van der Waals forces facilitate the adhesion of the bacteria to the surfaces of the particles. In addition, the bacteria may become attached to the particles through electrostatic interactions [34]. The surface charges of the bacteria and filter medium can be described by the point of zero charge (pHPZC), which is the pH value at which the external surface

Table 2
Column experimental results and transport model parameters for bacteria removal in dolomite

Exp.	m_{total} (mg)	q_{total} (mg)	Re (%)	q_0 (mg/g)	v_i (cm/min)	D_i (cm ² /min)	λ (1/min)	D_a	R^2
1	300	171.6 ± 2.9	57.2 ± 1.0	0.998 ± 0.019	0.093	0.757	0.0017	0.359	0.995
2	600	273.2 ± 11.4	45.5 ± 1.9	1.589 ± 0.072	0.179	0.599	0.0028	0.316	0.997
3	1,320	365.7 ± 11.7	27.7 ± 0.9	2.126 ± 0.067	0.215	0.634	0.0014	0.134	0.992
4	300	225.7 ± 10.0	75.2 ± 1.6	1.315 ± 0.062	0.063	0.177	0.0011	0.361	0.999
5	900	330.5 ± 0.9	36.7 ± 0.1	1.922 ± 0.009	0.198	1.088	0.0019	0.190	0.998
6	600	136.7 ± 4.0	22.8 ± 0.6	1.706 ± 0.051	0.182	0.392	0.0022	0.123	0.991
7	600	365.3 ± 14.7	60.9 ± 2.4	1.427 ± 0.058	0.166	0.451	0.0029	0.524	0.997

charge of the particles is zero. The pHPZC of a bacterium depends on the composition of the acid and base groups such as ammonium, carboxyl, phosphate, and sulfate groups on the cell surfaces, along with the adsorption of specific ions present in the aqueous phase on the cell surfaces. Above pH 3.0, the bacterial surface is generally negatively charged [35]. Therefore, at neutral pH, the surfaces of bacterial cells are negatively charged. For instance, *B. subtilis* is negatively charged above pH 2.1 [36]. The pHPZC of dolomite is 8.0 [37], the surface charge of dolomite under the current experimental conditions was slightly positive or neutral. Note that the pH of the effluent solution was equal to or below 8.0 (Table 1). Therefore, electrostatic interactions between the bacteria and dolomite may be active in the removal of bacteria from the solution by adhesion to dolomite.

The removal of bacteria by dolomite could also be affected by the elemental composition of dolomite. It is well known that teichoic acids on the cell walls of Gram-positive bacterial membranes bind strongly to Ca²⁺ and Mg²⁺ [38]. Note that teichoic acids are bacterial polysaccharides of glycerol phosphate or ribitol phosphate linked via phosphodiester bonds. Teichoic acid peptidoglycan on the cell wall of *B. subtilis* has been reported by Zheng et al. [2] to bind metal ions and Mg²⁺ in particular. Thus, Mg²⁺ ions present on the surface of dolomite may serve as the sorption sites for bacterial adhesion. In addition, Ca²⁺ and Mg²⁺ in the aqueous phase may enhance bacterial removal by the formation of bridges between bacteria adhered to the dolomite surface and free suspended bacteria in the aqueous phase. Foppen et al. [39] reported that addition of Ca²⁺ and Mg²⁺ to solution decreased the competitive effect of dissolved organic matter on the attachment of bacteriophages to goethite via cation bridging.

3.3. Application of kinetic models

Four kinetic models were applied to the BTCs obtained from the column experiments. Adams–Bohart,

Thomas, Yoon–Nelson, and dose–response models were used to simulate the BTCs and to estimate the basic parameters related to column design on a real scale. The theoretical BTCs are illustrated in Fig. 6 along with the experimental curves (Exps. 1, 4, and 7). The model parameters obtained from the model fittings for Exps. 1–7 are provided in Table 3. The Adams–Bohart model provided an adequate fit of the initial part of the experimental BTCs under all of the evaluated experimental conditions. The Thomas and Yoon–Nelson models were suitable for description of the transient stage of the BTCs between the breakthrough point and the saturation point. Compared to the aforementioned models, the dose–response model provided a relatively good simulation of the entire BTCs.

Several researchers [30,40,41] reported that the Adams–Bohart model is valid for relative concentrations below 0.15. In this study, the simulation of the initial part of the curves by fitting the experimental BTCs to the Adams–Bohart model provided a good fit of the theoretical BTCs for the relative concentration range up to 0.3, after which the theoretical curves increased sharply, with divergence from the experimental BTCs (Fig. 6). The rate constant (k_{AB}) and saturation concentration (N_0) were determined (Table 3) from the Adams–Bohart model and indicated that k_{AB} increased with increasing flow rate and decreasing column length. A higher flow rate and shorter column length increased the slope of the BTCs, thereby giving rise to higher k_{AB} values. The experimental values of N_0 increased with increasing influent concentration of bacteria and flow rate, whereas there was a decrease with increasing column length. The N_0 values calculated from the Adams–Bohart model deviated from the experimental values. The values of SSE obtained from the Adams–Bohart model ranged from 0.011 to 0.039, which were the lowest values from the four models used; the coefficients of determination (R^2) were higher than 0.9. It should be noted that despite the higher accuracy of the Adams–Bohart model as indicated by the smaller SSE and higher R^2 , the model

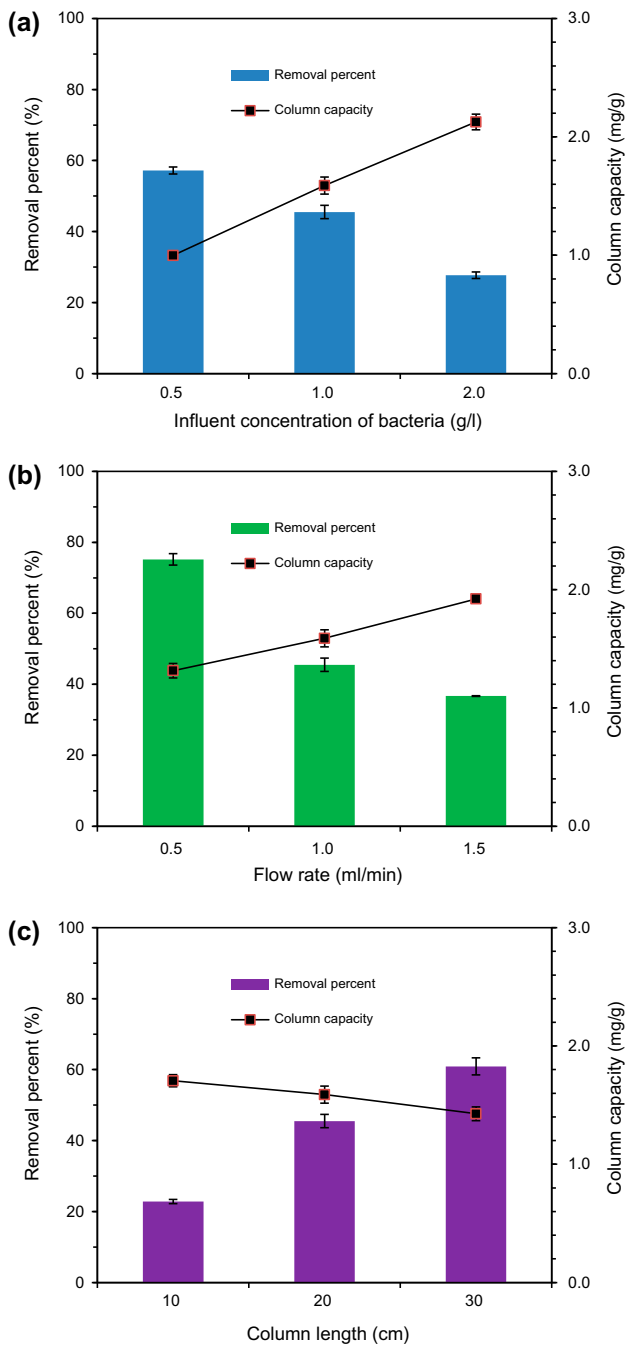


Fig. 5. Percentage bacterial removal and column capacity obtained from column experiments with variations of (a) influent bacterial concentration; (b) flow rate; (c) column length.

could only be applied for a low concentration of effluent. As stated, in the current study, the Adams–Bohart model adequately reproduced the initial part ($<0.3 C_t/C_0$) of the BTCs obtained under all of the evaluated experimental conditions.

The Thomas model was also fitted to the experimental BTCs (Fig. 6). The Thomas model is usually

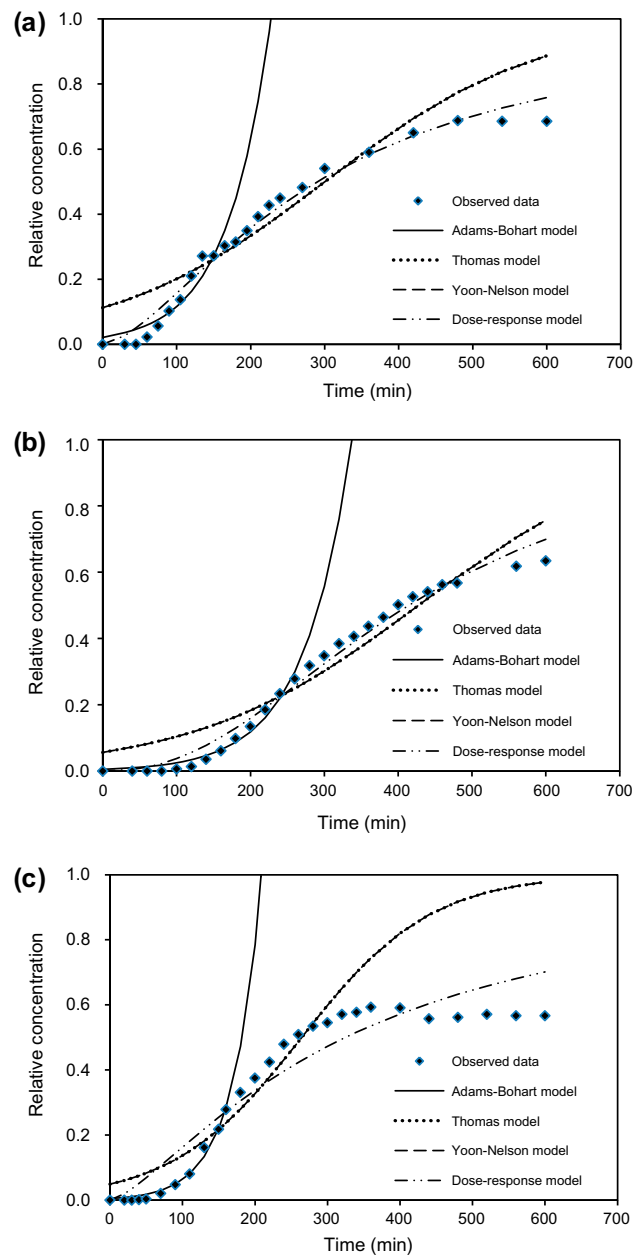


Fig. 6. Experimental and theoretical breakthrough curves from Adams–Bohart, Thomas, Yoon–Nelson, and dose-response kinetic models (Yoon–Nelson and Thomas model curves are superimposed): (a) Exp. 1; (b) Exp. 4; (c) Exp. 7. Kinetic model parameters are provided in Table 3.

applied to the relative concentration region between the breakthrough point and saturation point [23]. The rate constant (k_{Th}) and column capacity (q_0) were determined from the Thomas model (Table 3) and showed that the values of k_{Th} increased with increasing flow rate, whereas they decreased with increasing column length, similar to the trend in k_{AB} in the

Table 3
Kinetic model parameters obtained by nonlinear analysis of Adams–Bohart, Thomas, Yoon–Nelson, and dose–response models

Exp.	Adams–Bohart model					Thomas model				
	k_{AB} (L/mg/min)	$N_{0,cal}$ (mg/L)	$N_{0,exp}$ (mg/L)	R^2	SSE	k_{Th} (L/mg/min)	$q_{0,cal}$ (mg/g)	$q_{0,exp}$ (mg/g)	R^2	SSE
1	3.38E–05	1157.7	342.5	0.906	0.039	1.38E–05	0.884	0.998	0.912	0.057
2	3.87E–05	1285.6	706.0	0.969	0.019	1.47E–05	0.918	1.589	0.900	0.060
3	3.42E–05	1872.3	1764.0	0.982	0.021	0.78E–05	1.270	2.126	0.839	0.089
4	1.55E–05	1719.5	634.0	0.973	0.017	0.66E–05	1.257	1.315	0.848	0.091
5	5.32E–05	1455.9	807.0	0.974	0.017	1.71E–05	1.183	1.922	0.887	0.083
6	6.64E–05	1310.6	876.0	0.995	0.011	2.37E–05	0.839	1.706	0.834	0.095
7	2.53E–05	1422.8	571.0	0.985	0.013	1.12E–05	1.016	1.427	0.922	0.057
Yoon–Nelson model										
	k_{YN} (1/min)	τ_{cal} (min)	τ_{exp} (min)	R^2	SSE	Dose–response model				
						A	$q_{0,cal}$ (mg/g)	$q_{0,exp}$ (mg/g)	R^2	SSE
1	0.0069	300.4	280	0.912	0.057	1.577	0.844	0.998	0.982	0.033
2	0.0147	156.1	140	0.900	0.060	1.546	0.987	1.589	0.908	0.078
3	0.0155	108.0	95	0.839	0.089	2.068	1.236	2.126	0.958	0.066
4	0.0066	427.5	400	0.848	0.091	2.279	1.205	1.315	0.985	0.029
5	0.0171	134.0	117	0.887	0.083	1.453	1.180	1.922	0.962	0.059
6	0.0237	67.2	57	0.834	0.095	1.688	0.867	1.706	0.939	0.071
7	0.0112	264.3	252	0.922	0.057	1.391	1.269	1.427	0.913	0.073

Adams–Bohart model. The experimental values of q_0 increased with increasing bacterial influent concentration and flow rate, but decreased with increasing column length. The theoretical values ($q_{0,cal}$) were smaller than the experimental values ($q_{0,exp}$) for all of the stated experimental conditions. This could be attributed to the fact that the theoretical BTCs lie at higher relative concentrations than (i.e., were above) the experimental curves.

The curves derived from the Yoon–Nelson model were superimposed on the curves derived from the Thomas model (Fig. 6), given that the Yoon–Nelson model is mathematically analogous to the Thomas model. However, the Yoon–Nelson model gives different information describing the column behavior. The rate constant (k_{YN}) and the time required for 50% breakthrough of bacteria (τ) were calculated from the Yoon–Nelson model (Table 3). The values of k_{YN} increased with increasing bacterial influent concentration and flow rate, but decreased with increasing column length. The experimental values of τ decreased with increasing bacterial influent concentration and increased with increasing column length. The theoretical values (τ_{cal}) were higher than the experimental values (τ_{exp}) for all experimental conditions. This could be ascribed to the fact that the theoretical breakthrough points occurred earlier than the experimental ones.

The SSE values derived from the Thomas and Yoon–Nelson models ranged from 0.057 to 0.095, whereas the coefficients of determination (R^2) were between 0.834 and 0.922. In the region from low relative concentration to the upper saturation point, there was a divergence of the theoretical BTCs from the experimental values. The theoretical BTCs reached 1.0 at higher injection concentrations and flow rates, whereas the experimental BTCs did not attain a value of unity. The discrepancies between the experimental and theoretical BTCs occurred at higher flow rates and influent concentrations.

The theoretical BTCs derived from the dose-response model were in reasonably good agreement with the experimental values (Fig. 6). The SSE values calculated from the dose-response model ranged from 0.029 to 0.078 and the coefficients of determination (R^2) were higher than 0.9. The constant (A) and column capacity (q_0) were calculated from the dose-response model and the values of A decreased with increasing flow rate and column length. Similar to the Thomas model, the theoretical values ($q_{0,cal}$) obtained from the dose-response model were smaller than the experimental values ($q_{0,exp}$) under all evaluated experimental conditions.

4. Conclusions

Column experiments were conducted to investigate the removal of bacteria from aqueous solution by adsorption onto dolomite at various influent bacterial concentrations, flow rates, and column lengths. The results demonstrated that the percentage of bacterial removal decreased, whereas the column capacity increased, as the influent bacterial concentration and flow rate increased. The percentage removal increased with increasing column length, whereas the column capacity decreased. Theoretical analyses also indicated that the Adams–Bohart model provided an adequate reproduction of the initial part of the BTC, whereas the Thomas and Yoon–Nelson models were suitable for describing the transient stage of the BTCs between the breakthrough point and saturation point. Compared to the aforementioned models, the dose-response model produced an acceptable simulation of the entire BTC profile. This study demonstrates the adequate performance of dolomite as a filter material for the removal of bacteria from aqueous solution.

Acknowledgments

This work was supported by the project entitled “Development of Sustainable Remediation Technology for Marine Contaminated Sediments” funded by the Ministry of Land, Transport, and Maritime Affairs, Korea.

References

- [1] X. Zheng, P.J. Arps, R.W. Smith, Adsorption of *Bacillus subtilis* to minerals: effect on the flotation of dolomite and apatite, *Process Metall.* 9 (1999) 127–136.
- [2] X.P. Zheng, P.J. Arps, R.W. Smith, Adhesion of two bacteria onto dolomite and apatite: their effect on dolomite depression in anionic flotation, *Int. J. Miner. Process.* 62 (2001) 159–172.
- [3] A.M. Elmahdy, S.E. El-Mofty, N.A. Abdel-Khalek, A.A. El-Midany, Impact of the adsorption of *Corynebacterium diphtheriae intermedius* bacteria on enhancing the separation selectivity of dolomite and apatite, *Adsorpt. Sci. Technol.* 29 (2011) 47–57.
- [4] D. Grasso, B.F. Smets, K.A. Strevett, B.D. Machinist, C.J. VanOss, R.F. Giese, W. Wu, Impact of physiological state on surface thermodynamics and adhesion of *Pseudomonas aeruginosa*, *Environ. Sci. Technol.* 30 (1996) 3604–3608.
- [5] J.B. Morrow, R. Stratton, H.H. Yang, B.F. Smets, D. Grasso, Macro- and manoscale observations of adhesive behavior for several *E-coli* strains (O157: H7 and environmental isolates) on mineral surfaces, *Environ. Sci. Technol.* 39 (2005) 6395–6404.
- [6] B.A. Hudsonbaruth, M.G. Seitz, Adsorption of select phenol derivatives by dolomite, *Environ. Pollut. B* 11 (1986) 15–28.
- [7] H. Roques, L. Nugrohojeudy, A. Lebugle, Phosphorus removal from waste-water by half-burned dolomite, *Water Res.* 25 (1991) 959–965.
- [8] H.A. Aziz, P.G. Smith, Removal of manganese from water using crushed dolomite filtration technique, *Water Res.* 30 (1996) 489–492.

- [9] P.V. Brady, H.W. Papenguth, J.W. Kelly, Metal sorption to dolomite surfaces, *Appl. Geochem.* 14 (1999) 569–579.
- [10] S. Karaca, A. Gurses, M. Ejder, M. Acikyildiz, Adsorptive removal of phosphate from aqueous solutions using raw and calcinated dolomite, *J. Hazard. Mater.* 128 (2006) 273–279.
- [11] C.A. Prochaska, A.I. Zouboulis, Removal of phosphates by pilot vertical-flow constructed wetlands using a mixture of sand and dolomite as substrate, *Ecol. Eng.* 26 (2006) 293–303.
- [12] G.M. Ayoub, M. Mehawej, Adsorption of arsenate on untreated dolomite powder, *J. Hazard. Mater.* 148 (2007) 259–266.
- [13] S. Kocaoba, Comparison of Amberlite IR 120 and dolomite's performances for removal of heavy metals, *J. Hazard. Mater.* 147 (2007) 488–496.
- [14] E. Pehlivan, A.M. Ozkan, S. Dinc, S. Parlayici, Adsorption of Cu^{2+} and Pb^{2+} ion on dolomite powder, *J. Hazard. Mater.* 167 (2009) 1044–1049.
- [15] H. Bilinski, B. Matkovic, D. Kralj, D. Radulovic, V. Vrankovic, Model experiments with CaO, MgO and calcinated dolomite for fluoride removal in a wet scrubbing system with sea-water in recirculation, *Water Res.* 19 (1985) 163–168.
- [16] R. Marouf, N. Khelifa, K. Marouf-Khelifa, J. Schott, A. Khelifa, Removal of pentachlorophenol from aqueous solutions by dolomitic sorbents, *J. Colloid Interface Sci.* 297 (2006) 45–53.
- [17] A. Ghaemi, M. Torab-Mostaedi, M. Ghannadi-Maragheh, Characterizations of strontium(II) and barium(II) adsorption from aqueous solutions using dolomite powder, *J. Hazard. Mater.* 190 (2011) 916–921.
- [18] G.M. Walker, G. Connor, S.J. Allen, Copper (II) removal onto dolomitic sorbents, *Chem. Eng. Res. Des.* 82 (2004) 961–966.
- [19] S.J. Park, S.B. Kim, K.W. Kim, Analysis of bacterial cell properties and transport in porous media, *J. Environ. Sci. Health Part A-Toxic/Hazard. Subst. Environ. Eng.* 45 (2010) 682–691.
- [20] N. Toride, F.J. Leij, M.Th. van Genuchten, The CXTFIT code for estimating transport parameters from laboratory or field tracer experiments, Research Report No. 137, US Salinity Laboratory, 1995.
- [21] S.B. Kim, H.C. Ha, N.C. Choi, D.J. Kim, Influence of flow rate and organic carbon content on benzene transport in a sandy soil, *Hydrol. Process.* 20 (2006) 4307–4316.
- [22] G.S. Bohart, E.Q. Adams, Some aspects of the behavior of charcoal with respect to chlorine, *J. Am. Chem. Soc.* 42 (1920) 523–544.
- [23] H.C. Thomas, Heterogeneous ion exchange in a flowing system, *J. Am. Chem. Soc.* 66 (1944) 1664–1666.
- [24] Y.H. Yoon, J.H. Nelson, Application of gas-adsorption kinetics. 1. A theoretical-model for respirator cartridge service life, *Am. Ind. Hyg. Assoc. J.* 45 (1984) 509–516.
- [25] G.Y. Yan, T. Viraraghavan, M. Chen, A new model for heavy metal removal in a biosorption column, *Adsorpt. Sci. Technol.* 19 (2001) 25–43.
- [26] M.A. Martin-Lara, F. Hernainz, G. Blazquez, G. Tenorio, M. Calero, Sorption of Cr (VI) onto olive stone in a packed bed column: Prediction of kinetic parameters and breakthrough curves, *J. Environ. Eng.* 136 (2010) 1389–1397.
- [27] B.K. Shahraki, B. Mehrabi, R. Dabiri, Thermal behavior of Zefreh dolomite mine (central Iran), *J. Min. Metall.* 45B (2009) 35–44.
- [28] J. Ji, Y. Ge, W. Balsam, J.E. Damuth, J. Chen, Rapid identification of dolomite using a Fourier Transform Infrared Spectrophotometer (FTIR): A fast method for identifying Heinrich events in IODP site U1308, *Mar. Geol.* 258 (2009) 60–68.
- [29] S. Gunasekaran, G. Anbalagan, Thermal decomposition of natural dolomite, *Null. Mater. Sci.* 30 (2007) 339–344.
- [30] Z. Aksu, F. Gonen, Biosorption of phenol by immobilized activated sludge in a continuous packed bed: Prediction of breakthrough curves, *Process Biochem.* 39 (2004) 599–613.
- [31] R.P. Han, D.D. Ding, Y.F. Xu, W.H. Zou, Y.F. Wang, Y.F. Li, L. Zou, Use of rice husk for the adsorption of congo red from aqueous solution in column mode, *Bioresour. Technol.* 99 (2008) 2938–2946.
- [32] T.A. Camesano, B.E. Logan, Influence of fluid velocity and cell concentration on the transport of motile and nonmotile bacteria in porous media, *Environ. Sci. Technol.* 32 (1998) 1699–1708.
- [33] S.J. Park, C.G. Lee, S.B. Kim, Y.Y. Chang, J.K. Yang, Bacterial removal in flow-through columns packed with iron-manganese bimetallic oxide-coated sand, *J. Environ. Sci. Health Part A-Toxic/Hazard. Subst. Environ. Eng.* 47 (2012) 1364–1371.
- [34] A.T. Poortinga, R. Bos, W. Norde, H.J. Busscher, Electric double layer interactions in bacterial adhesion to surfaces, *Surf. Sci. Rep.* 47 (2002) 3–32.
- [35] H.H.M. Rijnaarts, W. Norde, J. Lyklema, A.J.B. Zehnder, The isoelectric point of bacteria as an indicator for the presence of cell-surface polymers that inhibit adhesion, *Colloid Surf. B-Biointerfaces* 4 (1995) 191–197.
- [36] Z.N. Hong, X.M. Rong, P. Cai, W. Liang, Q.Y. Huang, Effects of temperature, pH and salt concentrations on the adsorption of *Bacillus subtilis* on soil clay minerals investigated by microcalorimetry, *Geomicrobiol. J.* 28 (2011) 686–691.
- [37] O.S. Pokrovsky, J. Schott, F. Thomas, Dolomite surface speciation and reactivity in aquatic systems, *Geochim. Cosmochim. Acta* 63 (1999) 3133–3143.
- [38] M.T. Madigan, J.M. Martinko, Chapter 4. Cell structure and function, in: Brock Biology of Microorganisms, 11th ed., Pearson Education, New Jersey, 2006.
- [39] J.W.A. Foppen, S. Oklety, J.F. Schijven, Effect of goethite coating and humic acid on the transport of bacteriophage PRD1 in columns of saturated sand, *J. Contam. Hydrol.* 85 (2006) 287–301.
- [40] Y. Sag, Y. Aktay, Application of equilibrium and mass transfer models to dynamic removal of Cr(VI) ions by Chitin in packed column reactor, *Process Biochem.* 36 (2001) 1187–1197.
- [41] M. Calero, F. Hernainz, G. Blazquez, G. Tenorio, M.A. Martin-Lara, Study of Cr (III) biosorption in a fixed-bed column, *J. Hazard. Mater.* 171 (2009) 886–893.